Dimensional Synthesis of a Spatial Orientation 3-DoF Parallel Manipulator by Characterizing the Configuration Space

M. Urízar, V. Petuya, M. Diez, and A. Hernández

Abstract In this paper the authors approach the dimensional synthesis of parallel manipulators focusing on the evaluation of important entities belonging to the configuration space, such as workspace and joint space. In particular, 3-DoF manipulators that can perform non-singular transitions are considered, illustrating the procedure with a case study. The target is to search for designs that achieve the goals of adequate size and shape of the workspace.

Key words: Parallel manipulator, Configuration space, Dimensional Synthesis.

1 Introduction

In the design process of parallel manipulators several criteria have been presented in the literature for evaluating which architecture is best. Designers often search for the optimum design parameters such that certain important requirements are achieved. From the kinematic point of view, optimal design methodologies are principally focused on: workspace [6, 8, 2], kinematic performance indices [3, 1], task development [7], etc. Features such as workspace and dexterity can be emphasized as two significant considerations [5, 1], because parallel manipulators have relative smaller workspaces and complex singularities compared to their serial counterparts.

The analysis of the singularity loci, together with the distribution of the Direct Kinematic Problem (DKP) solutions over the workspace, has received a lot of attention during the last years. In this field, the phenomenon of *assembly mode change*, also known as *non-singular solution change*, has been extensively studied [11, 4, 10]. It consists in analyzing how the transitions between different DKP solutions can be made in a safety and controlled way. Manipulators presenting this

M. Urízar, V. Petuya, M. Diez and A. Hernández
University of the Basque Country, Faculty of Engineering in Bilbao, Mechanical Engineering Dpt.
Alameda de Urquijo s/n, 48013 Bilbao (Spain), e-mail: monica.urizar@ehu.es

ability can enlarge their range of motion, as they have access to all the regions associated with the solutions involved in the transition. However, it must be emphasized that, usually, not all the designs of the same manipulator own this ability.

In this paper, the dimensional synthesis of this type of manipulators is approached by characterizing entities of the configuration space, such as workspace and joint space. For three-degree-of-freedom parallel manipulators these entities that can be represented in a three-dimensional space. So as to show the procedure the spatial orientation 3-SPS-S parallel manipulator is used as an illustrative example. This manipulator has a broad range of applications, such as: orienting a tool or a workpiece, solar panels, space antennas, camera devices, human wrist prosthesis, haptic devices, etc. The purpose is to analyze several designs, assessing the influence of the design parameters on the resultant workspace and joint space. Then, the aim is to search for the set of possible designs that best satisfy the requirements of size and shape of the operational workspace.

2 Case study: 3-SPS-S parallel manipulator

The spatial orientation 3-SPS-S parallel manipulator shown in Fig. 1a will be studied. The 3-SPS-S manipulator is made up of a moving platform $OB_1B_2B_3$, a base platform $OA_1A_2A_3$, and three extensible limbs denoted by l_i. Both platforms take the form of a tetrahedron, connected one to each other by a fixed spherical joint at point O. The robot has 3-DoF (ϕ, θ, ψ) defining the orientation of the moving platform.

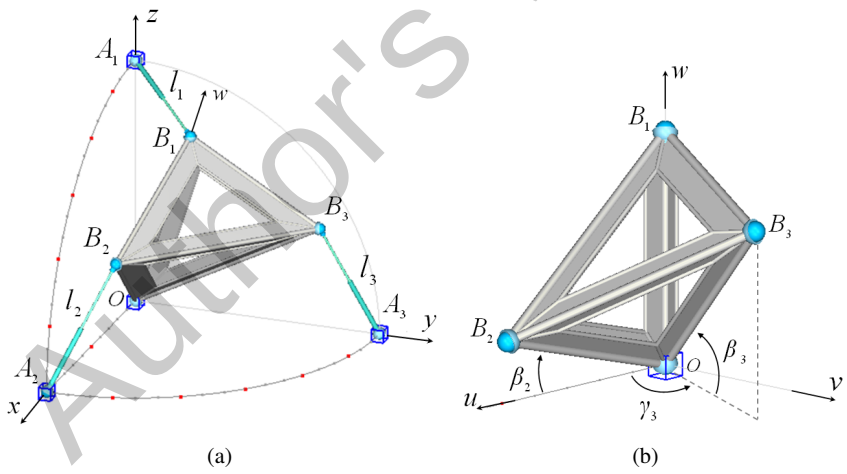

Fig. 1: (a) Spatial 3-SPS-S parallel manipulator; (b) Design parameters of the moving platform

With respect to the base platform, the fixed spherical joints A_i are located on the principal axes of the fixed frame $\mathscr{F}\{\mathbf{x},\mathbf{y},\mathbf{z}\}$ fulfilling $|\overrightarrow{OA_i}| = R$, for $i = 1,2,3$. Besides, the spherical joints B_i are located with respect to the moving frame $\mathscr{M}\{\mathbf{u},\mathbf{v},\mathbf{w}\}$ (see Fig. 1b) such that:

$$\begin{aligned} {}^{\mathscr{M}}\mathbf{b}_1 &= L[0,0,1]^T \\ {}^{\mathscr{M}}\mathbf{b}_2 &= L[b_{2u},0,b_{2w}]^T \\ {}^{\mathscr{M}}\mathbf{b}_3 &= L[b_{3u},b_{3v},b_{3w}]^T \end{aligned} \tag{1}$$

where

$$\begin{aligned} &b_{2u} = c\beta_2; \qquad b_{2v} = 0; \qquad b_{2w} = s\beta_2 \\ &b_{3u} = c\beta_3 c\gamma_3; \quad b_{3v} = c\beta_3 s\gamma_3; \quad b_{3w} = s\beta_3 \end{aligned} \tag{2}$$

The transformation from the moving frame $\mathscr{M}$ to the fixed frame $\mathscr{F}$ can be achieved by a 3×3 rotation matrix ${}^{\mathscr{F}}_{\mathscr{M}}\mathbf{R}$ defined by the three Euler angles. In this case, the Euler angles (ϕ,θ,ψ) in their **wvw** version will be used.

The vector ${}^{\mathscr{F}}\mathbf{b}_i$, or simply $\mathbf{b}_i$, expressed with respect to the fixed frame $\mathscr{F}$ is:

$$\mathbf{b}_i = [b_{ix},b_{iy},b_{iz}]^T = {}^{\mathscr{F}}_{\mathscr{M}}\mathbf{R}\,{}^{\mathscr{M}}\mathbf{b}_i \tag{3}$$

On the other hand, the position vector of points A_i with respect to the fixed frame $\mathscr{F}$ is $\mathbf{a}_i = [a_{ix},a_{iy},a_{iz}]^T$.

The loop-closure equation for each limb is $\mathbf{l}_i = \mathbf{b}_i - \mathbf{a}_i$, which results in the following system for $i = 1,2,3$:

$$l_i^2 = \mathbf{a}_i^2 + \mathbf{b}_i^2 - 2\mathbf{a}_i^T\mathbf{b}_i \tag{4}$$

- *Inverse Kinematic Problem*: To solve the IKP, the Euler angles are established (ϕ,θ,ψ) and the length of each limb l_i can be directly obtained from Eq. 4. Only the positive solution yields a physical meaning.
- *Direct Kinematic Problem*: The DKP consists in solving the outputs (ϕ,θ,ψ) once the three prismatic limb lengths are known. As demonstrated in [9] this manipulator has a maximum of eight solutions to the DKP.

2.1 Velocity Problem

So as to solve the velocity problem the loop-closure equations are differentiated with respect to time, obtaining:

$$\boldsymbol{\omega}_p \times \mathbf{b}_i = \boldsymbol{\omega}_i \times \mathbf{l}_i + \dot{l}_i \cdot \mathbf{s}_i \tag{5}$$

where $\mathbf{s}_i$ is defined as the unit vector directed from A_i to B_i. The moving platform angular velocity is ω_p, and ω_i corresponds to the angular velocity of each limb l_i. Dot-premultiplying each term of the system (5) by $\mathbf{l}_i$, the velocity equation expressed in a matrix form is obtained as:

$$\mathbf{J}_{DKP}\left\{\omega_p\right\} = \mathbf{J}_{IKP}\left\{\dot{l}_i\right\} \tag{6}$$

where

$$\mathbf{J}_{DKP} = \begin{bmatrix} (\mathbf{b}_1 \times \mathbf{l}_1)^T \\ (\mathbf{b}_2 \times \mathbf{l}_2)^T \\ (\mathbf{b}_3 \times \mathbf{l}_3)^T \end{bmatrix}; \quad \mathbf{J}_{IKP} = \begin{bmatrix} l_1 & 0 & 0 \\ 0 & l_2 & 0 \\ 0 & 0 & l_3 \end{bmatrix} \tag{7}$$

The inverse Jacobian matrix, $\mathbf{J}_{IKP}$, is singular only whenever any of the prismatic limbs has zero length, which cannot be achieved in practice. Besides, each limb has only one associated working mode. Hence, we focus on the analysis of the DKP singularity locus in the configuration space.

2.2 DKP Singularity Locus

The DKP singularity locus is obtained by computing the nullity of the determinant of $\mathbf{J}_{DKP}$, which yields:

$$|\mathbf{J}_{DKP}| = -R^3L^3 \cdot s\theta \cdot \xi \tag{8}$$

where

$$\begin{aligned} \xi = {} & c^2\phi c\theta(b_{2w}(b_{3u}s\psi + b_{3v}c\psi) - b_{3w}(b_{2u}s\psi)) - c^2\phi s\theta(b_{3v}b_{2u}) \\ & + c^2\psi s\theta(b_{2u}b_{3v}) + s\theta(c\psi s\psi(b_{2u}b_{3u})) - c\theta(b_{2w}(b_{3u}s\psi + b_{3v}c\psi)) \\ & + s\phi c\phi(b_{2w}(b_{3u}c\psi - b_{3v}s\psi) - b_{3w}b_{2u}c\psi) \end{aligned} \tag{9}$$

Expression $|\mathbf{J}_{DKP}|$ factorizes into three terms:

- The constant R^3L^3 does not affect the shape of the DKP singularity locus. Parameters R and L define the size of the robot, and the minimum and maximum stroke of the prismatic limbs. For the example under study, without loss of generality, values $R = 1$ and $L = 0.5$ will be assigned.
- The second term corresponds to the function: $s\theta$. So as to avoid the singularity planes $\theta = 0$ and $\theta = \pm\pi$, the interval $\theta \in (0, \pi)$ will be considered.
- Finally, from Eq. 9 yields the expression ξ. This function depends on the output variables (ϕ, θ, ψ), and on the geometric parameters $(\beta_2, \gamma_3, \beta_3)$. Therefore, the expression ξ will be assessed regarding the dimensional synthesis.

3 Dimensional Synthesis

Parameters $(\beta_2, \gamma_3, \beta_3)$ comprise the design parameters subject of study. Different designs will be analyzed, representing and assessing workspace and joint space entities.

- **Case 1**: Similar Platforms

The first case under study establishes a design of the moving platform such that it is similar to the fixed base. For that, the geometric parameters are: $\beta_2 = \beta_3 = 0$ and $\gamma_3 = 90^\circ$. The expression of the DKP singularity locus, given by Eq. 9, yields:

$$\xi = s\theta(c\psi - c\phi)(c\psi + c\phi) \tag{10}$$

It is factorized into the function $s\theta$, and the product of two planes. These planes divide the workspace (ϕ, θ, ψ) into eight aspects, so $V_{case1} = V_T/8$ being V_T the total volume. Each DKP solution lies inside each aspect, non-singular transitions being not possible. This is corroborated with the non-existence of cusp points inside any section of the joint space (see details in [9], chapter 10).

- **Case 2**: Joints B_2, B_3 on **uv**-plane

The second case under study locates joints B_2 and B_3 on the **uv**-plane, such that $\beta_2 = \beta_3 = 0$ and γ_3 varies in the interval $(0, 90^\circ)$. The DKP singularity locus yields:

$$\xi = s\theta[b_{3u}s\psi c\psi + b_{3v}(c^2\psi - c^2\phi)] \tag{11}$$

Yet again, expression ξ factorizes into the function $s\theta$, and a trigonometric expression depending on outputs (ϕ, ψ) and coordinates b_{3u} and b_{3v}, function of the geometric parameter γ_3. Let us analyze a design included in Case 2, by assigning $\gamma_3 = 30^\circ$. The DKP singularity locus is represented in the workspace in Fig. 2a, the joint space and its cross section for $l_1 = const$ being depicted in Fig. 2b. Contrary to Case 1, only four aspects exist, so that the operational workspace is duplicated $V_{case2} = 2V_{case1} = V_T/4$, because the robot can move between solutions located inside the same aspect. This is in accordance with the existence of cusp points in joint space sections, as shown in Fig. 2b.

Non-singular transitions can be performed between regions in the workspace where different solutions lie, as for example regions 1 and 2 in the workspace section of Fig. 2c. Though the size of the workspace is $V_T/4$ for all designs in Case 2, its shape varies. It is interesting to search for designs that yield a regular workspace, such that the range of motion of the output variables maintains over the entire workspace. As shown in Fig. 2c, the ratio $H = h/r$ can be measured and serves as an indicator of regularity. Its evolution depending on γ_3 is represented in Fig. 2d. It can be observed that small values of γ_3 yield a more regular workspace ($H \approx 1$). The extreme values $\gamma_3 = 0$ (planar moving platform) and $\gamma_3 = 90^\circ$ constitute particular designs. On the one hand, $\gamma_3 = 0$ yields a degeneracy design for which the workspace is formed by planes ($H = 1$) and only 4 DKP solutions exist.

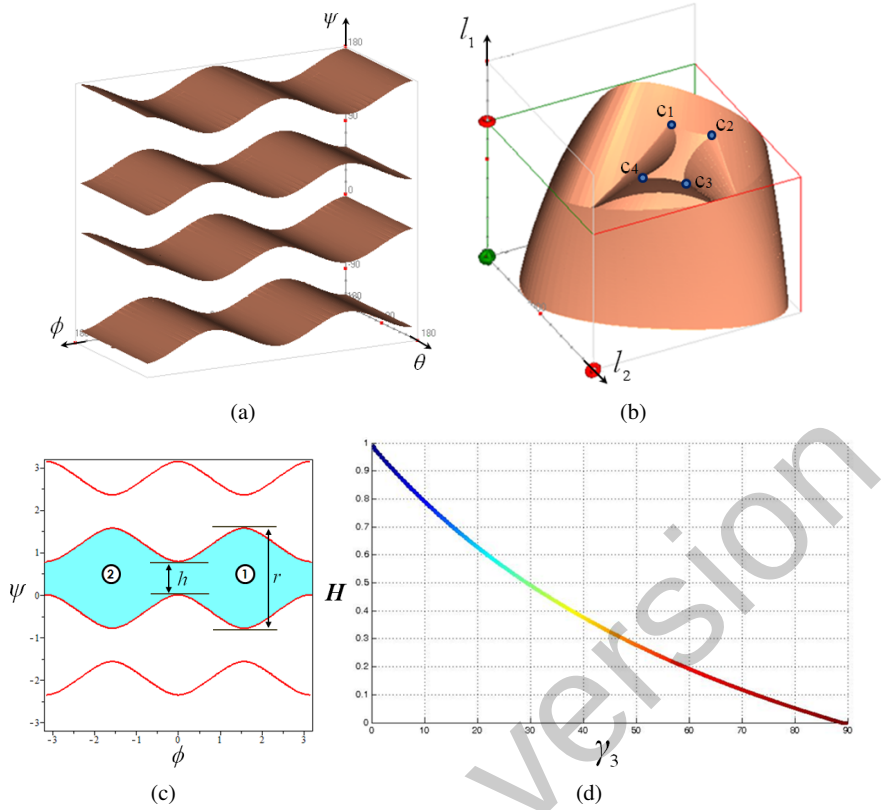

Fig. 2: Case 2: DKP singularity locus in the (a) workspace, (b) joint space and (c) workspace section;(d) Ratio of regularity H

Value $\gamma_3 = 90°$ coincides with Case 1, and verifies $H = 0$, no connection between different regions is possible.

- **Case 3**: General Design

The last case corresponds to a general design of the moving platform. For this case the three dimensional parameters $(\beta_2, \gamma_3, \beta_3)$ can be assigned any value in the range $(0, 90°)$. The singularity locus is given by expression ξ in Eq. (9), which is plotted in the workspace and joint space in Fig. 3 for a specific design: $\beta_2 = 30°$, $\gamma_3 = 60°$ and $\beta_3 = 30°$. Some sections of the joint space are also depicted in Fig. 3b, visualizing the existence of cusp points.

These designs present two aspects, the holes of the singularity surface in the workspace (Fig. 3a) allowing the connection between all solutions having the same sign of $|\mathbf{J}_{DKP}|$. Consequently, the designs of Case 3 exhibit the maximum operational workspace: $V_{case3} = V_T/2$. Nevertheless, the shape that the singularity surface acquires in the workspace, and in the joint space, is much more complex.

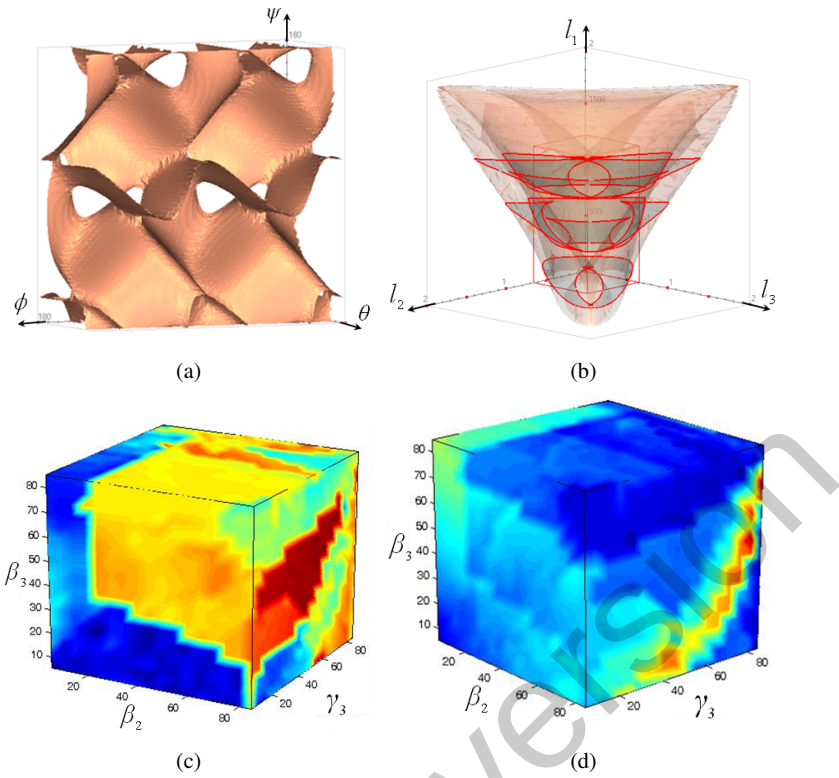

Fig. 3: Case 3: DKP singularity locus in the (a) workspace and (b) joint space; Design parameter space according to indicators (c) R_1 and (d) R_2

In this sense, similarly to Case 2, some indicators that characterize the shape of the operational workspace can be implemented. Then, parameters $(\beta_2, \gamma_3, \beta_3)$ comprise the *design parameter space* in which each point represents a possible design, and has an associated value according to the indicator under evaluation. We propose two indicators. The first, R_1, evaluates the regularity, comparing the number of nodes forming the DKP singularity curves among different sections of $\theta_i \in (0, \pi)$. The second indicator, R_2, assesses the quality of the curves in each θ_i section, penalizing the designs for which the curves cover a larger region. The results are displayed in Figs. 3c and 3d, the blue colored points indicate the geometric parameters corresponding to optimum designs, and the red ones the worst (see details in [9]).

The optimum design parameter space can be computed by intersecting the optimum values of both graphs in Figs. 3c and 3d. Then, any point belonging to the resultant optimum space constitutes a valid design complying with the established requirements. For example, the following design: $\beta_2 = 15°$, $\gamma_3 = 10°$ and $\beta_3 = 20°$ is an optimum design with regular workspace, maintaining a similar pattern of the singularity curves in different sections of the workspace.

4 Conclusions

Dimensional synthesis of a spatial orientation manipulator has been approached, focusing mainly on the configuration space entities. Analyzing different designs, it has been shown that the ones capable of transitioning between solutions exhibit a larger workspace. Not only the size of the operational workspace but the evaluation of its shape has been also considered, representing the design parameter space according to the different requirements. Then the designer can choose any point belonging to the set of optimum values achieved. The proposed procedure is valid for 3-DoF planar or spatial parallel manipulators that exhibit the transitioning ability.

Acknowledgment

The authors wish to acknowledge the financial support received from Ministerio de Economía y Competitividad (Project DPI2011- 22955), the European Union (Project FP7-CIP-ICT-PSP-2009-3) and Basque Government, Dpto. Educ., Univ. e Investig. (Project IT445-10) and UPV/EHU under program UFI 11/29.

References

1. Altuzarra, O., Pinto, C., Sandru, B., Hernández, A.: Optimal Dimensioning for Parallel Manipulators: Workspace, Dexterity and Energy. ASME Journal of Mechanical Design **133(4)**, 041,007–7 (2011)
2. Bonev, I., Rhyu, J.: A geometrical method for computing the constant-orientation workspace of 6-PRRS parallel manipulators. Mechanism and Machine Theory **36**, 1–13 (2001)
3. Gosselin, C., Angeles, J.: A global performance index for the kinematic optimization of robotic manipulators. Journal of Mechanical Design **113(3)**, 220–226 (1991)
4. Husty, M.: Non-singular assembly mode change in 3-RPR-parallel manipulators. In: Computational Kinematics, (Eds. Kecskeméthy, A., Müller, A), Springer (2009)
5. Liu, X.J., Guan, L., Wang, J.: Kinematics and Closed Optimal Design of a Kind of PRRRP Parallel Manipulator. ASME Journal of Mechanical Design **129(5)**, 558563. (2007)
6. Merlet, J.P.: Designing a parallel manipulator for a specific workspace. International Journal of Robotics Research **16(4)**, 545–556 (1997)
7. Monsarrat, B., Gosselin, C.: Workspace Analysis: and Optimal Design of a 3-Leg 6-DOF Parallel Platform Mechanism. IEEE Trans. on Robotics and Automation **19(6)**, 954–966 (2003)
8. Ottaviano, E., Ceccarelli, M.: An Analytical Design for CaPaMan with Prescribed Position and Orientation. In: Proc. of the ASME Design Engineering Technical Conference and Computers and Information in Engineering Conference, Baltimore (2000)
9. Urízar, M.: Methodology to Enlarge the Workspace of Parallel Manipulators by Means of Non-singular Transitions. Ph.D. thesis, University of the Basque Country (UPV/EHU). http://www.ehu.es/compmech/members/monica-urizar/research/ (2012)
10. Urízar, M., Petuya, V., Altuzarra, O., Hernández, A.: Assembly Mode Changing in the Cuspidal Analytic 3-RPR. IEEE Transactions on Robotics **28(2)**, 506–513 (2012)
11. Zein, M., Wenger, P., Chablat, D.: Non-singular assembly mode changing motions for 3-RPR parallel manipulators. Mechanism and Machine Theory **43 (4)**, 480–490 (2008)